Focus, Guide and Alignment system for DESI

Han Soul Lee
Florida Atlantic University
Wayne State University Physics REU 2014
SLAC National Laboratory
Advisor: Dr. Kevin Reil

Dark Energy Spectroscopic Instrument(DESI), which is planned to be installed on the Kitt Peak Observatory, Tuscon, Arizona in 2018 is a project seeking to map the 3D model of the universe. The model is created through obtaining precise measurement the red shifts and Baryon acoustic oscillations from the astronomical object. Once the light is received to the instrument's fiber-tips, the spectrum is analyzed and the redshift by calculated. By obtaining the object's distance from earth, the instrument allows to model three dimensional model of the universe. This research was conducted for guide, focus and alignment system for DESI.

1. Background

The GFA (Guide, Focus and Alignment system) for DESI is consist of 10 cameras. The DESI focal surface consists of 10 “petals” each with 500 fiber tips and one GFA camera. Once the light enters the fiber, the spectrum is analyzed and obtains the wavelength which calculates redshift. The camera will be running at ambient temperature, where the dark current noise is expected to be increased sharply with the temperature. Unfortunately, the CCD camera with the desired e2v sensor did not arrived in time. Rather an alternative CCD camera produced by Santa Barbara Instrument Group (SBIG) camera was used for test performance instead. In addition to dark current studies, stellar density analysis images were taken from Blanco telescope in Chile. The Blanco telescope is an identical to Mayall telescope in Tuscon, Arizona which DESI will be mounted. A single exposure was taken at 8

different galactic latitudes (each exposure has62 sensors). Two of the sensors (number two and sixty one) are known to have problems, and thus data from those sensors were excluded from the analysis process. To confirm Mayall telescope's ability to obtain accurate measures of astronomical objects, exposures from Blanco's were used to compare the number of the star counts per galactic magnitudes to existing NOMAD catalog.

2. Procedure

Since 60 sensors took individual exposures for each parts of the galactic location, each location required total combined result of 60 images. In order to extract only stars from each images, Source Extractor (shortened as SExtractor) was used as a main program for the research. Once the sextractor had returned the output catalog, the catalog was once again filtered to leave only objects with higher possibilities of being stars. Using the updated catalog, a region file was created. The region file was then applied onto the applicable fits file to ds9. Each image was carefully examined through ds9 to confirm the most accurate results. Once the stars were extracted from each exposure, a MAG_AUTO histogram was created to compare the pattern with other exposures in the same extensions. A final histogram that total all the stars in each RA and DEC was later created. Ultimately, the number of stars per magnitude in each galactic latitude which was compared to the results found in NOMAD catalog.

3. Process

The dark current from the SBIG camera was measured from taking dark exposures in different temperature. The ranged from -12 to 20 celsius. Five minute exposures were taken for each temperature. From the exposure, average pixel values

were measured and compared.

Sextractor version 2.8.6 was installed for stellar analysis purposes, which was later updated to version 2.19.7. Shell script was written to run sextractor on the individual images consecutively. The sextracted results were returned as a catalog for each individual images, which contained detected objects. The catalog also contained personalized parameter values, such as MAG_AUTO, Ellipticity and FLAG. The catalogs often included objects with variety of errors such as saturated and blended stars. The biggest challenge though the process was to omit the saturated stars from the catalog.

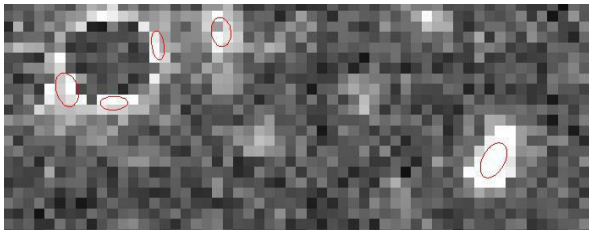

Figure 1. A black and round object on the top left corner is a saturated star

A black spot on the top left corner in figure 1 demonstrates an example of a saturated star. Saturation, caused by the over flow of photon in the in particular area appears as a black donuts with bright rim. Each of the images contained different saturation level which pixels arises saturation value. In order to assign correct saturation level for each image, sextractor required default.sex file with each personalized saturation level. To personalize default.sex script, which contained different required parameter values for sextraction, pyfits's header function was used to reach the individual saturation level in the header. Once the saturated stars were omitted from the catalog, another issue was raised where the program started to include parts of the rim as an elongated individual objects. From figure 1, ellipses around the saturated star is located around the spot on the top left corner. On the

bottom right corner an elongated object (suspected to be a galaxy) is also included in the catalog as well. Stars are round gaseous objects. Since it appears as a round object, returned ellipticity was used to filter the objects with lower possibility to be stars. Equation for ellipticity follows:

$$e = 1 - \frac{B}{A}$$

Where A is the major axis and B is the minor axis of an ellipse. As B increases to the value of A, the limit of e reaches zero. Thus rounder the object, ellipticity closer to zero. After filtering the images for different values of ellipticity, 0.25 returned the best results.

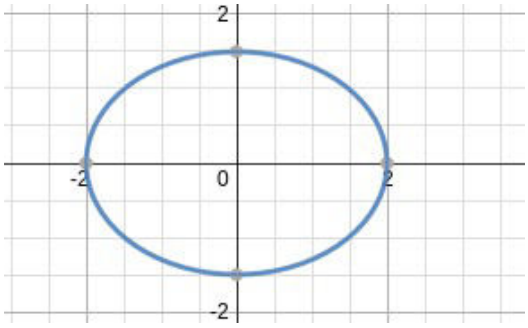

Figure 2, an eplise with ellipticity 0.25

1	The object has neighbours, bright and close enough to significantly bias the MAG_AUTO photometry[13], or bad pixels (more than 10% of the integrated area affected),
2	The object was originally blended with another one,
4	At least one pixel of the object is saturated (or very close to),
8	The object is truncated (too close to an image boundary),
16	Object's aperture data are incomplete or corrupted,
32	Object's isophotal data are incomplete or corrupted[14],
64	A memory overflow occurred during deblending,
128	A memory overflow occurred during extraction.

Figure 3, list of flags value

In addition to the ellipticity, flags parameter, the value raised for any detection error was also used in filtering process. The filtration limit was set as 3. Any object with blending issue was eliminated from the analysis process. By eliminating objects with blending issue, saturation and elongation, approximate number of star count was obtained. Using the updated catalog, ds9 region file was created. The image of an exposure before and after filtration is shown below:

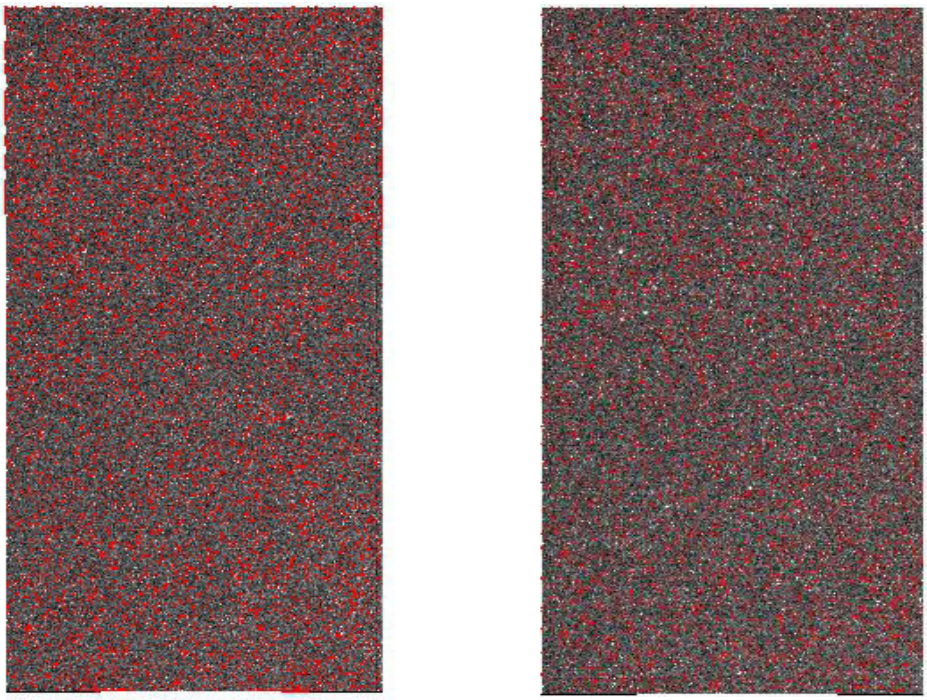

Figure 4, DECam00315141, 41st sensor *before* extraction(left) and *after* extraction(right)

Once the python script had filtered the objects, a new catalog with updated objects was created. The right image in figure 2's region file was created from the updated catalog. From the catalog, histograms for MAG_AUTO were created for 60 images in the same galactic coordinates. Before saving the graph into pdf file, individual graphs were manually viewed to confirm the consistent patterns between the graphs. Comparison between the individual histogram and galactic latitude is shown in figure 5 and 6 below:

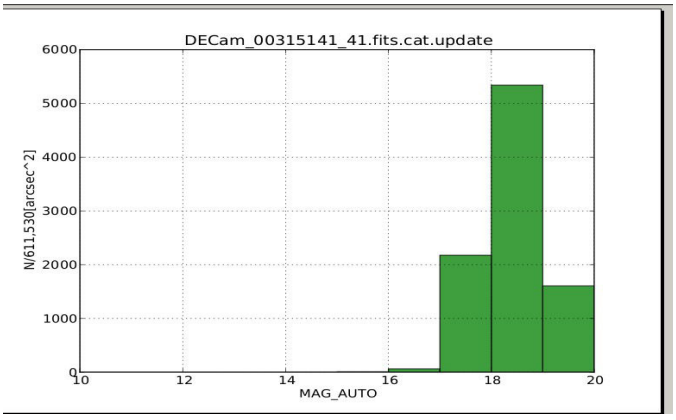

Figure 5. histogram of MAG_AUTO for sensor 41 in DECam_00315141

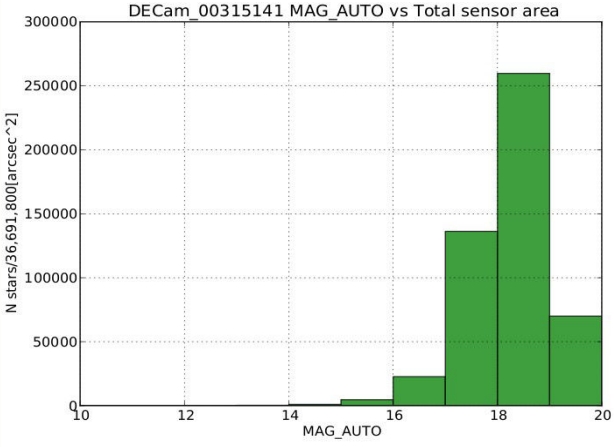

Figure 6. histogram of MAG_AUTO for all 60 sensor in DECam_00315141

The bin values ranged from 10 to 20. Very few stars were detected under bins

10 to 14. Stars in those bins are assumes to be unfiltered saturated stars. The number of stars in each bin increased in counts until bin 20, where the detection limit was reached. This is an expected pattern. As there are more distant stars from the Earth than nearby, there are more dim stars expected in the back ground than brighter stars.

Once the expected pattern was observed, all the values of the star's magnitude in 60 different images were appended into an array. The magnitude histograms of total stars in each galactic latitude was created (figure 6 above). Once the accurate counts of stars in different magnitude per latitude was obtained, the results were combined into a final plot. Before the plotting the graph, the size of the sensor needed to be calculated in dergee^2 instead of arcsec^2. The math is shown below:

$$PIXSCALE = 0.27\frac{arcsec}{pix}$$

$$x = 2048 \ \ pix$$

$$y = 4096 \ \ pix$$

$$x = 0.27[pix] \cdot 2048[\frac{arcsec}{pix}]$$

$$y = 0.27[pix] \cdot 4096[\frac{arcsec}{pix}]$$

$$x = 553arcsec$$

$$y = 1106arcsec$$

$$A = x \cdot y$$

$$A = 611618arcsec^2$$

$$60arcmin = 1degree$$

$$3600arcsec = 1degree$$

$$(3600)^2 arcsec^2 = degree^2$$

$$arcsec^2 = \frac{1}{(3600)^2} degree^2$$

$$A = \frac{611,618}{3600^2} = 0.047degree^2$$

By using the conversion factor, the N stars per latitude was recalculated, then log_10_(y) was applied to the final plot:

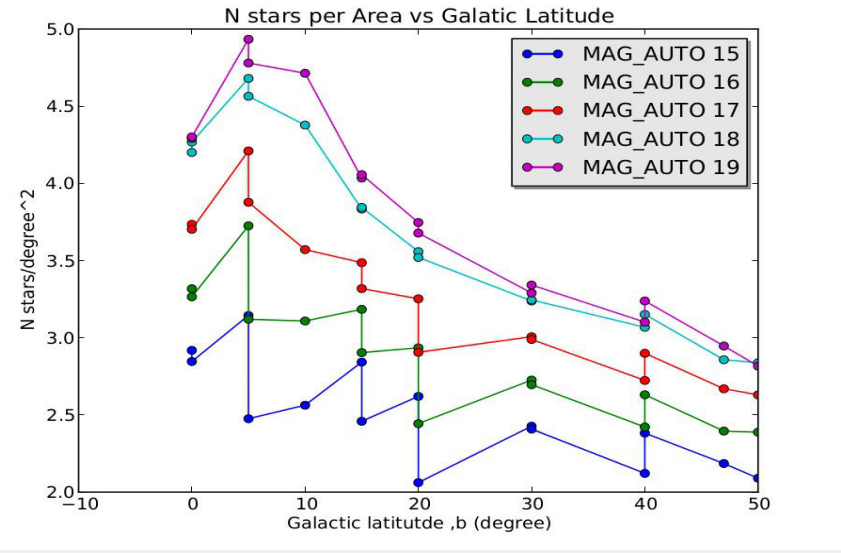

Figure 7, N stars vs Galactic Latitude plot

3. Results

The dark currents were measured as expected:

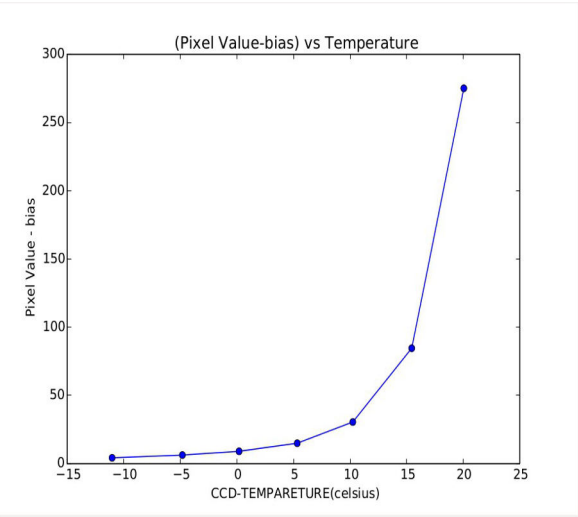

Figure 8, Pixel Value-bias vs Temperature

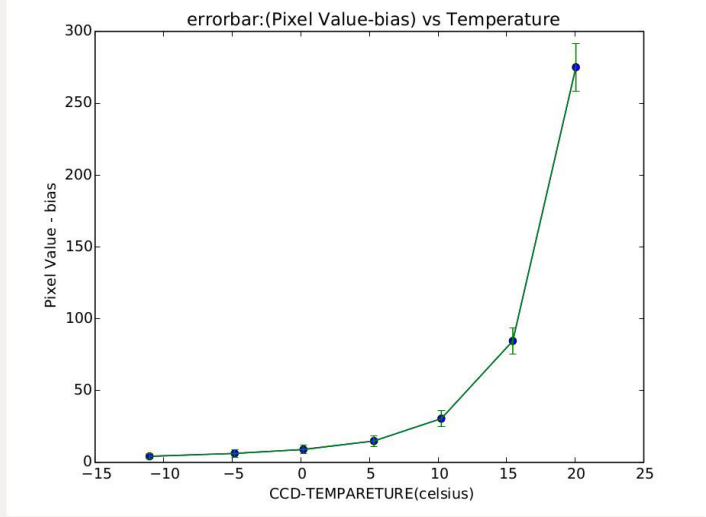

Figure 9, Pixel Value-bias vs Temperature with errorbar

The average pixel value increase with a factor every five degrees. As the temperature increased, the noise caused by generation of electron has increased. This is an expected results as the heat, higher energy has caused to generate more

electrons.

Three trends are observed from the graph in figure 7: 1. As the brightness of stars decreased, the slope of each graph becomes more stable and gradual. 2. The star counts peaked at b=5 degrees and decreased from there. 3. There are a sudden increase in star count between galactic latitude zero to five degrees.

The first two observed trends are expected. As mentioned earlier, there are more counts of dim stars than brighter stars in the background. Stars in brighter magnitude has smaller size of sample compared to dimmer stars. Although both magnitude 15 and 19 had both decreased in counts from b=5 to 50, slope of magnitude 15 has an inconsistent decrease rate; there are sudden decrease and increase in the plot until the count has reached b=50. It is interesting to notice that the pattern observed in magnitude 15 is conserved until it becomes gradually stabilized through out the magnitude. This is consistent with the logic; greater the sample, more apparent in the pattern. The random increase and decrease in brighter stars are due to lack of samples in brighter stars.

The last trend is explained through the appearance of the Milky Way galaxy. The exposures were taken from 13 different galactic latitudes in which 5 locations were very close to each other. The exact location of the exposures are as below:

l=10.0006, b=-0.001
l=359.9997, b=0.0006
l=10.0011, b=4.9985
l=10.0011, b=4.9985
l=359.9992, b=5.001
l=9.9993, b=10.0009
l=359.9991, b=15.0012
l=9.9988, b=15.0015
l=359.9992, b=20.0012
l=9.9991, b=20.0013

l=9.9999, b=30.0003
l=359.9995, b=30.0004
l=359.9993, b=40.0004
l=9.9991, b=40.0009
l=355.1904, b=46.9791

The sharp increase in N stars from b=0 to b=5 is explained from the image below:

Figure 8, Central Disk of the Milky Way Galaxy (image credit:NASA)

As observed from the image, the center of the galaxy is blocked by the tick band of medians across the center of the Milkey Way galaxy. As a result, there are significant decrease in the visible star count in the central disk region. Such result is consistent from the NOMAD catalog results:

l=0.0 b=-45.0 ra=320.3 dec=-41.7 n=2978

l=0.0 b=-40.0 ra=313.6 dec=-41.6 n=3299

l=0.0 b=-35.0 ra=306.9 dec=-41.2 n=4435

l=0.0 b=-30.0 ra=300.4 dec=-40.4 n=5884

l=0.0 b=-25.0 ra=294.1 dec=-39.2 n=7748

l=0.0 b=-20.0 ra=288.0 dec=-37.7 n=12515

l=0.0 b=-15.0 ra=282.2 dec=-35.9 n=25461

l=0.0 b=-10.0 ra=276.6 dec=-33.8 n=67299

l=0.0 b=-5.0 ra=271.4 dec=-31.5 n=115206

l=0.0 b=0.0 ra=266.4 dec=-29.0 n=25029

l=0.0 b=5.0 ra=261.6 dec=-26.3 n=78572

l=0.0 b=10.0 ra=257.1 dec=-23.5 n=58610

l=0.0 b=15.0 ra=252.7 dec=-20.5 n=14000

l=0.0 b=20.0 ra=248.6 dec=-17.4 n=9151

l=0.0 b=25.0 ra=244.5 dec=-14.3 n=5720

l=0.0 b=30.0 ra=240.6 dec=-11.1 n=3916

l=0.0 b=35.0 ra=236.8 dec= -7.8 n=3677

l=0.0 b=40.0 ra=233.0 dec= -4.5 n=2863

l=0.0 b=45.0 ra=229.2 dec= -1.2 n=2542

l=0.0 b=50.0 ra=225.5 dec= 2.2 n=2436

The final graph is confirmed from the above chart. As indicated from the graph, the patterns found in graphs are consistent through out the NOMAD catalog. The number of visible stars increase between galactic latitude 0 to 5 degrees, and decrease as away from the disk. The sharp decrease in galactic disk is very apparent. Although center of the disk is the most crowded region in the galaxy, by the stellar medians such as dust and other astronomical object's visible stars in the disk is very limited compared to the existing stars.

4. Conclusion

The Blanco in Chile is confirmed to be capable of detecting astronomical objects as we have expected. As the capacity has been confirmed, it is also concluded that Mayall Telescope in Kitt Peak observatory also has ability to detect the necessary astronomical objects. Mayall telescope is a suitable telescope for DESI to create the 3D model of the universe.